Acknowledgments

We thank Stefano Piccolo (Padova University) and Tomotoshi Marumoto (Kyushu University) for comments; Tomotoshi Marumoto, Hiroshi Yamada, and Koji Takei for gifts of materials; Hiroyuki Yanai and Takehiro Tanaka for pathologic assessment. We also thank Yumiko Morishita for the preparation of paraffin-embedded sections, Masumi Furutani for help with the electron microscopic study (Central Research Laboratory, Okayama University), and Ai Ueda for technical assistance in our laboratory (Okayama University).

References

[1] Wen PY and Kesari S (2008). Malignant gliomas in adults. *N Engl J Med* **359**, 492–507.

[2] Kaur B, Khwaja FW, Severson EA, Matheny SL, Brat DJ, and Van Meir EG (2005). Hypoxia and the hypoxia-inducible-factor pathway in glioma growth and angiogenesis. *Neuro Oncol* **7**, 134–153.

[3] Pàez-Ribes M, Allen E, Hudock J, Takeda T, Okuyama H, Viñals F, Inoue M, Bergers G, Hanahan D, and Casanovas O (2009). Antiangiogenic therapy elicits malignant progression of tumors to increased local invasion and distant metastasis. *Cancer Cell* **15**, 220–231.

[4] Rong Y, Durden DL, Van Meir EG, and Brat DJ (2006). 'Pseudopalisading' necrosis in glioblastoma: a familiar morphologic feature that links vascular pathology, hypoxia, and angiogenesis. *J Neuropathol Exp Neurol* **65**, 529–539.

[5] Brat DJ, Castellano-Sanchez AA, Hunter SB, Pecot M, Cohen C, Hammond EH, Devi SN, Kaur B, and Van Meir EG (2004). Pseudopalisades in glioblastoma are hypoxic, express extracellular matrix proteases, and are formed by an actively migrating cell population. *Cancer Res* **64**, 920–927.

[6] Ricci-Vitiani L, Pallini R, Biffoni M, Todaro M, Invernici G, Cenci T, Maira G, Parati EA, Stassi G, Larocca LM, et al. (2010). Tumour vascularization via endothelial differentiation of glioblastoma stem-like cells. *Nature* **468**, 824–828.

[7] Wang R, Chadalavada K, Wilshire J, Kowalik U, Hovinga KE, Geber A, Fligelman B, Leversha M, Brennan C, and Tabar V (2010). Glioblastoma stem-like cells give rise to tumour endothelium. *Nature* **468**, 829–833.

[8] Keunen O, Johansson M, Oudin A, Sanzey M, Rahim SA, Fack F, Thorsen F, Taxt T, Bartos M, Jirik R, et al. (2011). Anti-VEGF treatment reduces blood supply and increases tumor cell invasion in glioblastoma. *Proc Natl Acad Sci USA* **108**, 3749–3754.

[9] Méndez O, Zavadil J, Esencay M, Lukyanov Y, Santovasi D, Wang SC, Newcomb EW, and Zagzag D (2010). Knock down of HIF-1α in glioma cells reduces migration *in vitro* and invasion *in vivo* and impairs their ability to form tumor spheres. *Mol Cancer* **9**, 133.

[10] Marotta D, Karar J, Jenkins WT, Kumanova M, Jenkins KW, Tobias JW, Baldwin D, Hatzigeorgiou A, Alexiou P, Evans SM, et al. (2011). *In vivo* profiling of hypoxic gene expression in gliomas using the hypoxia marker EF5 and laser-capture microdissection. *Cancer Res* **71**, 779–789.

[11] Ragel BT, Couldwell WT, Gillespie DL, and Jensen RL (2007). Identification of hypoxia-induced genes in a malignant glioma cell line (U-251) by cDNA microarray analysis. *Neurosurg Rev* **30**, 181–187.

[12] Bennin DA, Don AS, Brake T, McKenzie JL, Rosenbaum H, Ortiz L, DePaoli-Roach AA, and Horne MC (2002). Cyclin G2 associates with protein phosphatase 2A catalytic and regulatory B′ subunits in active complexes and induces nuclear aberrations and a G_1/S phase cell cycle arrest. *J Biol Chem* **277**, 27449–27467.

[13] Arachchige Don AS, Dallapiazza RF, Bennin DA, Brake T, Cowan CE, and Horne MC (2006). Cyclin G2 is a centrosome-associated nucleocytoplasmic shuttling protein that influences microtubule stability and induces a p53-dependent cell cycle arrest. *Exp Cell Res* **312**, 4181–4204.

[14] Kim Y, Shintani S, Kohno Y, Zhang R, and Wong DT (2004). Cyclin G2 dysregulation in human oral cancer. *Cancer Res* **64**, 8980–8986.

[15] Adorno M, Cordenonsi M, Montagner M, Dupont S, Wong C, Hann B, Solari A, Bobisse S, Rondina MB, Guzzardo V, et al. (2009). A mutant-p53/Smad complex opposes p63 to empower TGFβ-induced metastasis. *Cell* **137**, 87–98.

[16] Montagner M, Enzo E, Forcato M, Zanconato F, Parenti A, Rampazzo E, Basso G, Leo G, Rosato A, Bicciato S, et al. (2012). SHARP1 suppresses breast cancer metastasis by promoting degradation of hypoxia-inducible factors. *Nature* **487**, 380–384.

[17] Marumoto T, Tashiro A, Friedmann-Morvinski D, Scadeng M, Soda Y, Gage FH, and Verma IM (2008). Development of a novel mouse glioma model using lentiviral vectors. *Nat Med* **15**, 110–116.

[18] Xu G, Bernaudo S, Fu G, Lee DY, Yang BB, and Peng C (2008). Cyclin G2 is degraded through the ubiquitin-proteasome pathway and mediates the anti-proliferative effect of activin receptor-like kinase 7. *Mol Biol Cell* **19**, 4968–4979.

[19] Aguilar V, Annicotte JS, Escote X, Vendrell J, Langin D, and Fajas L (2010). Cyclin G2 regulates adipogenesis through PPARγ coactivation. *Endocrinology* **151**, 5247–5254.

[20] Fujimura A, Michiue H, Nishiki T, Ohmori I, Wei FY, Matsui H, and Tomizawa K (2011). Expression of a constitutively active calcineurin encoded by an intron-retaining mRNA in follicular keratinocytes. *PLoS One* **6**, e17685.

[21] Puntervoll P, Linding R, Gemünd C, Chabanis-Davidson S, Mattingsdal M, Cameron S, Martin DM, Ausiello G, Brannetti B, Costantini A, et al. (2003). ELM server: a new resource for investigating short functional sites in modular eukaryotic proteins. *Nucleic Acids Res* **31**, 3625–3630.

[22] Kim SH, Park YY, Kim SW, Lee JS, Wang D, and DuBois RN (2011). ANGPTL4 induction by prostaglandin E_2 under hypoxic conditions promotes colorectal cancer progression. *Cancer Res* **71**, 7010–7020.

[23] Wolf A, Agnihotri S, Micallef J, Mukherjee J, Sabha N, Cairns R, Hawkins C, and Guha A (2011). Hexokinase 2 is a key mediator of aerobic glycolysis and promotes tumor growth in human glioblastoma multiforme. *J Exp Med* **208**, 313–326.

[24] Semenza GL, Jiang BH, Leung SW, Passantimo R, Concordet JP, Marie P, and Giallongo A (1996). Hypoxia response elements in the aldolase A, enolase 1, and lactate dehydrogenase A gene promoters contain essential binding sites for hypoxia-inducible factor 1. *J Biol Chem* **271**, 32529–32537.

[25] Martínez-Gac L, Marqués M, García Z, Campanero MR, and Carrera AC (2004). Control of cyclin G2 mRNA expression by forkhead transcription factors: novel mechanism for cell cycle control by phosphoinositide 3-kinase and forkhead. *Mol Cell Biol* **24**, 2181–2189.

[26] Fu G and Peng C (2011). Nodal enhances the activity of FoxO3a and its synergistic interaction with Smads to regulate cyclin G2 transcription in ovarian cancer cells. *Oncogene* **30**, 3953–3966.

[27] Lee CC, Jan HJ, Lai JH, Ma HI, Hueng DY, Lee YC, Cheng YY, Liu LW, Wei HW, and Lee HM (2010). Nodal promotes growth and invasion in human gliomas. *Oncogene* **29**, 3110–3123.

[28] Zilberberg L, Shinkaruk S, Lequin O, Rousseau B, Hagedorn M, Costa F, Caronzolo D, Balke M, Canron X, Convert O, et al. (2003). Structure and inhibitory effects on angiogenesis and tumor development of a new vascular endothelial growth inhibitor. *J Biol Chem* **278**, 35564–35573.

[29] Co C, Wong DT, Gierke S, Chang V, and Taunton J (2007). Mechanism of actin network attachment to moving membranes: barbed end capture by N-WASP WH2 domains. *Cell* **128**, 901–913.

[30] Singh VP and McNiven MA (2008). Src-mediated cortactin phosphorylation regulates actin localization and injurious blebbing in acinar cells. *Mol Biol Cell* **19**, 2339–2347.

[31] Feng H, Liu KW, Guo P, Zhang P, Cheng T, McNiven MA, Johnson GR, Hu B, and Cheng SY (2012). Dynamin 2 mediates PDGFRα-SHP-2-promoted glioblastoma growth and invasion. *Oncogene* **31**, 2691–2702.

[32] Oser M, Yamaguchi H, Mader CC, Bravo-Cordero JJ, Arias M, Chen X, Desmarais V, van Rheenen J, Koleske AJ, and Condeelis J (2009). Cortactin regulates cofilin and N-WASp activities to control the stages of invadopodium assembly and maturation. *J Cell Biol* **186**, 571–587.

[33] Mader CC, Oser M, Magalhaes MA, Bravo-Cordero JJ, Condeelis J, Koleske AJ, and Gil-Henn H (2011). An EGFR-Src-Arg-Cortactin pathway mediates functional maturation of invadopodia and breast cancer cell invasion. *Cancer Res* **71**, 1730–1741.

[34] Kruchten AE, Krueger EW, Wang Y, and McNiven MA (2008). Distinct phospho-forms of cortactin differentially regulate actin polymerization and focal adhesions. *Am J Physiol Cell Physiol* **295**, C1113–C1122.

[35] Lu KV, Zhu S, Cvrljevic A, Huang TT, Sarkaria S, Ahkavan D, Dang J, Dinca EB, Plaisier SB, Oderberg I, et al. (2009). Fyn and Src are effectors of oncogenic epidermal growth factor receptor signaling in glioblastoma patients. *Cancer Res* **69**, 6889–6898.

[36] Du J, Bernasconi P, Clauser KR, Mani DR, Finn SP, Beroukhim R, Burns M, Julian B, Peng XP, Hieronymus H, et al. (2009). Bead-based profiling of tyrosine kinase phosphorylation identifies SRC as a potential target for glioblastoma therapy. *Nat Biotechnol* **27**, 77–83.

[37] Liu BA, Jablonowski K, Raina M, Arcé M, Pawson T, and Nash PD (2006). The human and mouse complement of SH2 domain proteins—establishing the boundaries of phosphotyrosine signaling. *Mol Cell* **22**, 851–868.

[38] Tian L, Chen L, McClafferty H, Sailer CA, Ruth P, Knaus HG, and Shipston MJ (2006). A noncanonical SH3 domain binding motif links BK channels to the actin cytoskeleton via the SH3 adapter cortactin. *FASEB J* **20**, 2588–2590.

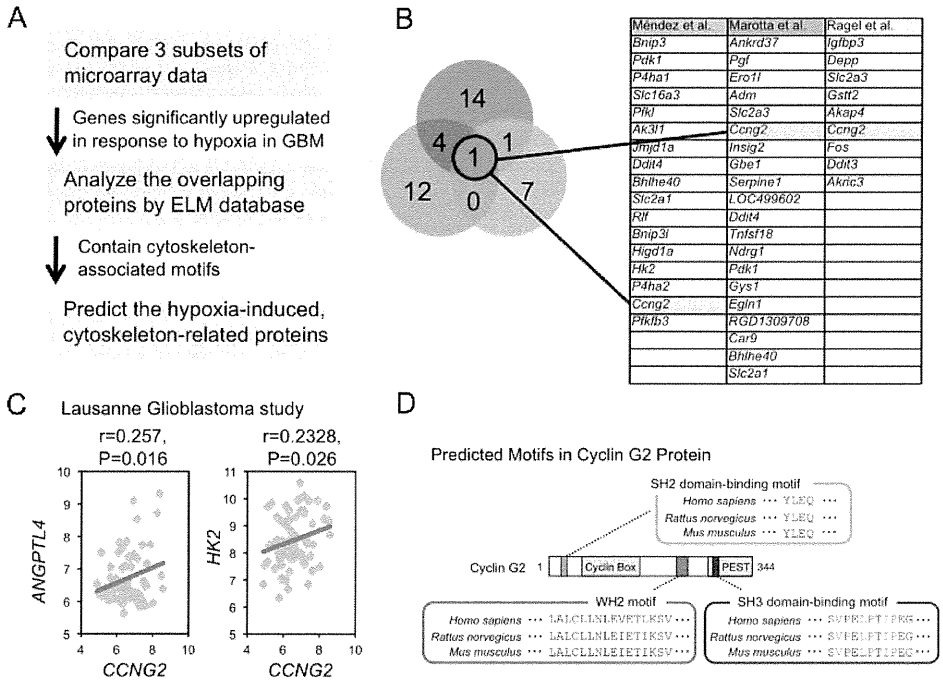

Figure W1. (A) Diagram of the procedure to predict the hypoxia-induced and cytoskeleton-associated proteins in human glioma cell lines. (B) *Cyclin G2* is a commonly upregulated gene in response to hypoxia among three subsets of microarray data of glioblastoma study. (C) The expression level of cyclin G2 is correlated with hypoxia-responsive genes, *ANGPTL4* and *HK2*, in Lausanne glioblastoma study (Accession ID: GSE7696). (D) The ELM database predicts that cyclin G2 protein has a putative SH2 or SH3 domain–binding motif and WH2 motif.

Figure W2. The human cyclin G2 promoter region contains putative HREs. The human cyclin G2 promoter region (−1600~0) contains some putative HREs (-CGTG-; red) and a FoxO3a-binding site (blue). The transcription starting site (underlined in shaded sequence) and the translation initiating ATG (boxed) were determined according to NCBI (Accession No. NM 004354.2).

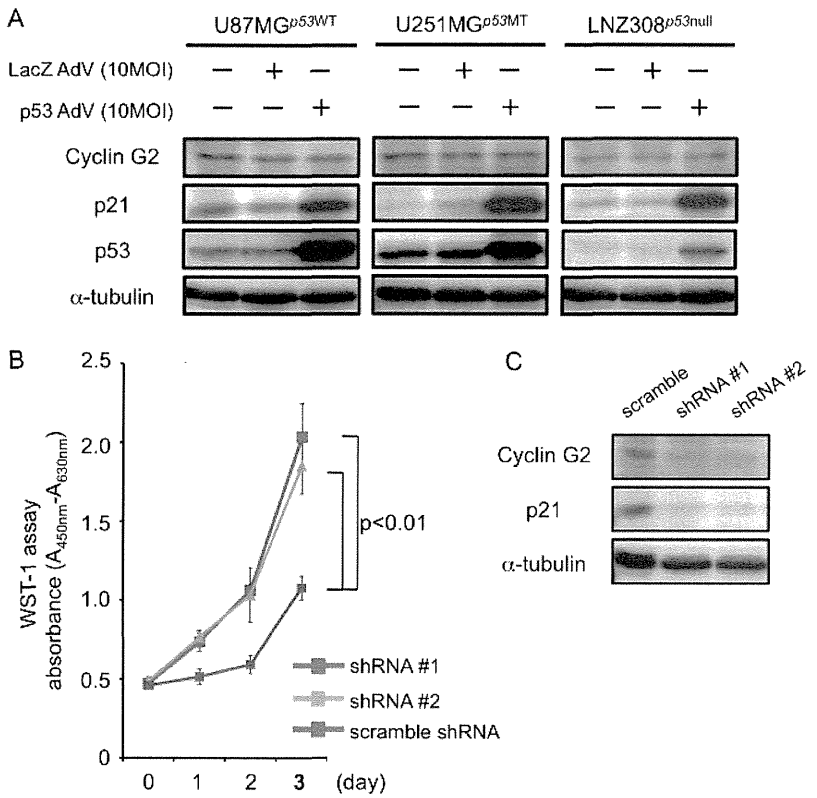

Figure W3. (A) Western blot analyses of U87MG ($p53^{WT}$), U251MG ($p53^{Mut}$), and LNZ308 ($p53^{Null}$) cells infected with *lacZ* or p53 adenovirus. These results show that the level of p53 does not affect that of cyclin G2 and forced expression of p53 does not induce cyclin G2 expression in GBM. (B) WST-1 assay showing the effect of cyclin G2's reduction on cell-cycle regulation in U87MG cells. (C) Cyclin G2 reduction resulted in p21 suppression.

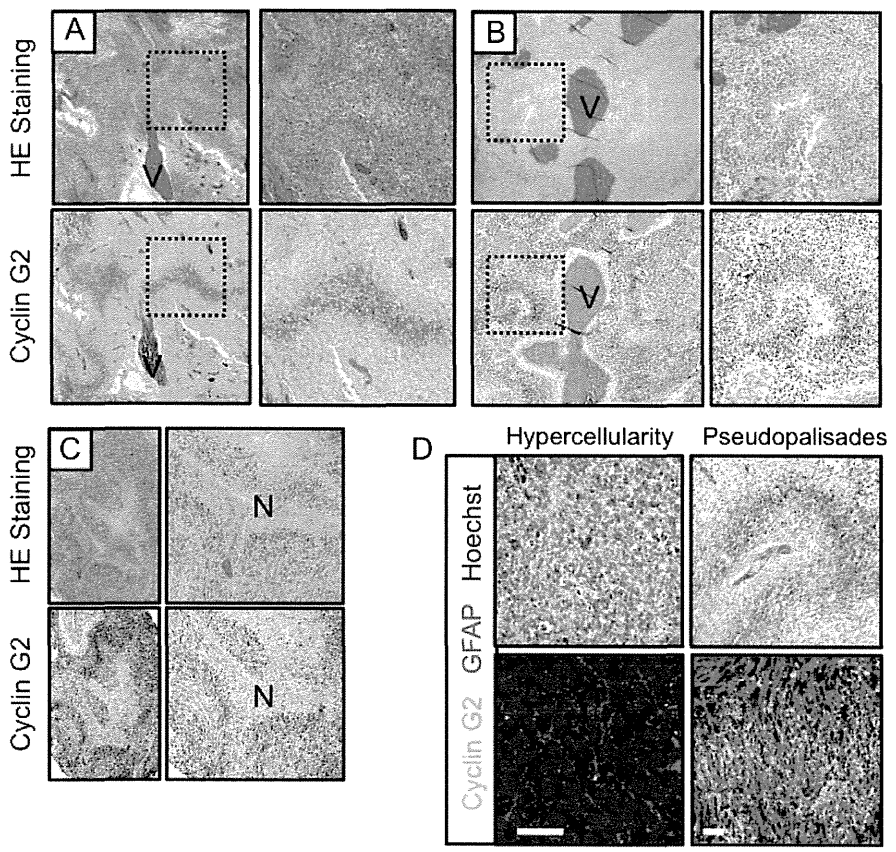

Figure W4. Cyclin G2 is abundant in pseudopalisade-forming glioma cells. (A–C) Cyclin G2 expression in pseudopalisades is observed in various types of GBM specimens. (D) Cyclin G2 is absent in high cellularity/high mitotic regions in GBM. The scale bars represent 10 μm in D. "V" and "N" indicate vessel and necrosis, respectively.

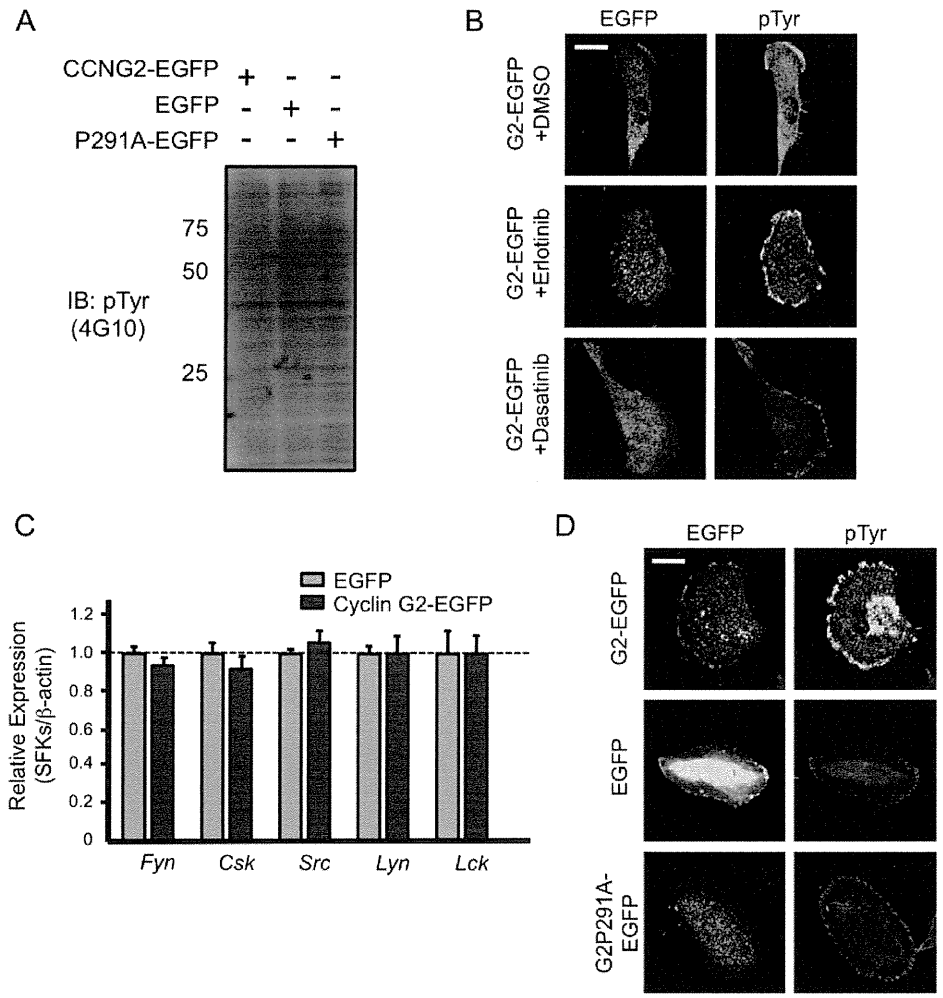

Figure W5. Cyclin G2 induces the restricted tyrosine phosphorylation of cortactin in an SFK-dependent manner. (A) Ectopic expression of cyclin G2 does not alter the total amount of tyrosine phosphorylation. (B) Dasatinib inhibits the phosphorylation induced by cyclin G2. Note that dasatinib, but not erlotinib, decreases the peripheral signals of phosphotyrosine induced by cyclin G2. The scale bar represents 10 μm in B. (C) Cyclin G2 does not enhance transcription of SFK mRNA. (D) Exogenous cyclin G2 increases, whereas the P291A mutant impairs, tyrosine phosphorylation signals at the juxtamembrane. The scale bar represents 10 μm in D.

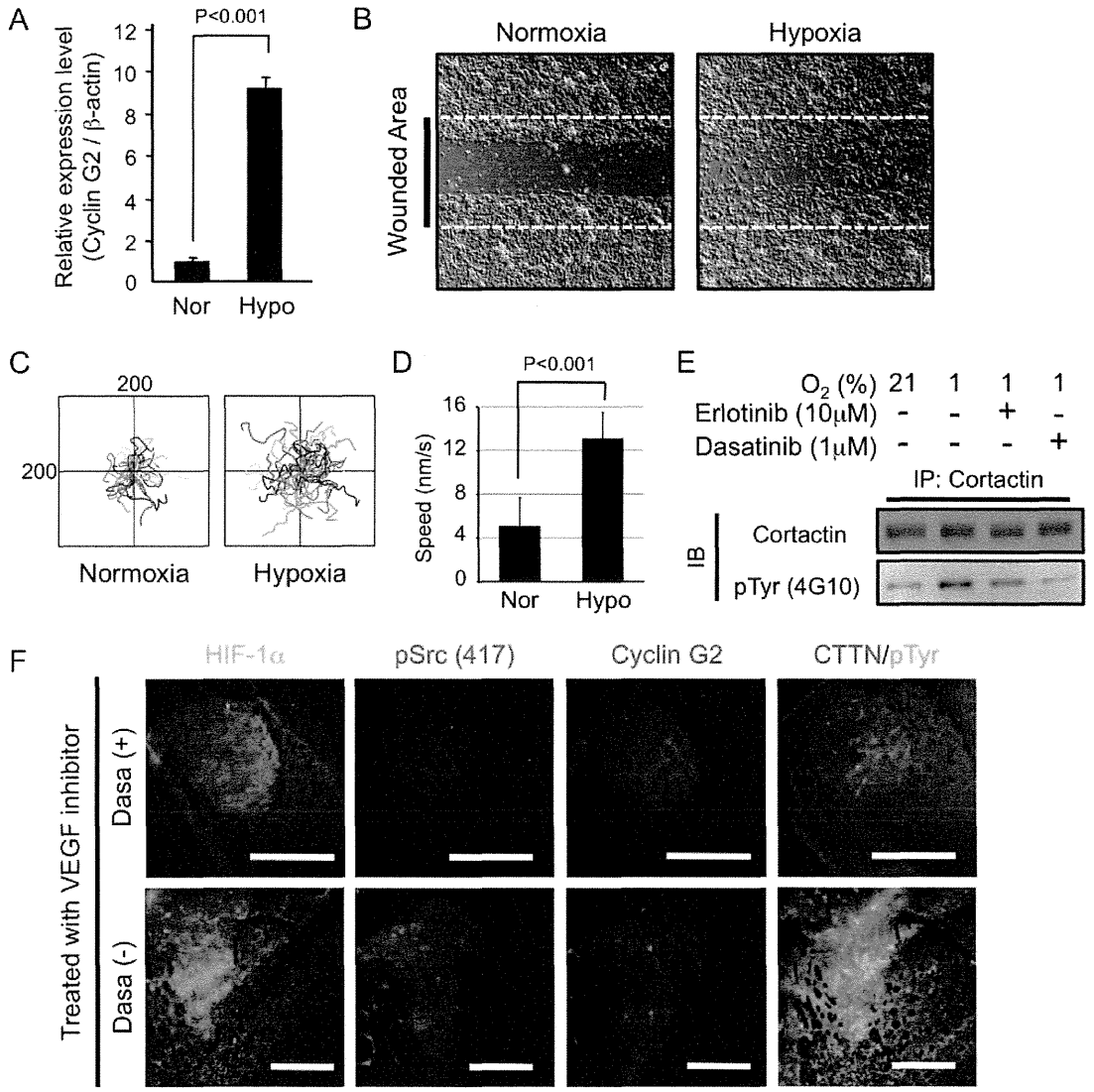

Figure W6. The effectiveness of dasatinib on the expansion of glioma-initiating cells. (A) Cyclin G2 expression is enhanced in response to hypoxia in murine glioma-initiating 005 cells. (B–D) Hypoxia stimulates the motility of 005 cells. (E) Tyrosine phosphorylation of cortactin is enhanced in response to hypoxic stimulation in 005 cells and dasatinib attenuates it. Note that 005 cells show the phosphorylation in a normoxic and steady state. (F) Dasatinib attenuates the hypoxia-driven local invasion of 005 cells. Note that dasatinib treatment inhibits the phosphorylation of src and cortactin. The scale bars represent 200 μm (F).

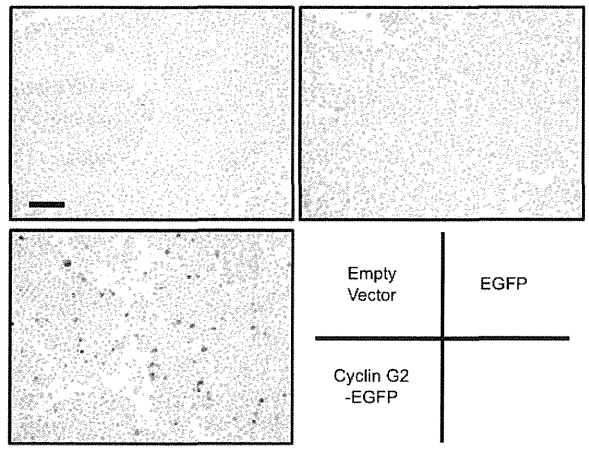

Figure W7. Goat anti-human cyclin G2 antibody (Santa Cruz Biotechnology, Inc) successfully recognized ectopic cyclin G2 in paraffin-embedded HEK293 cells that were transfected with cyclin G2–EGFP. For other applications including immunoblot analysis, see references. The scale bar represents 100 μm.

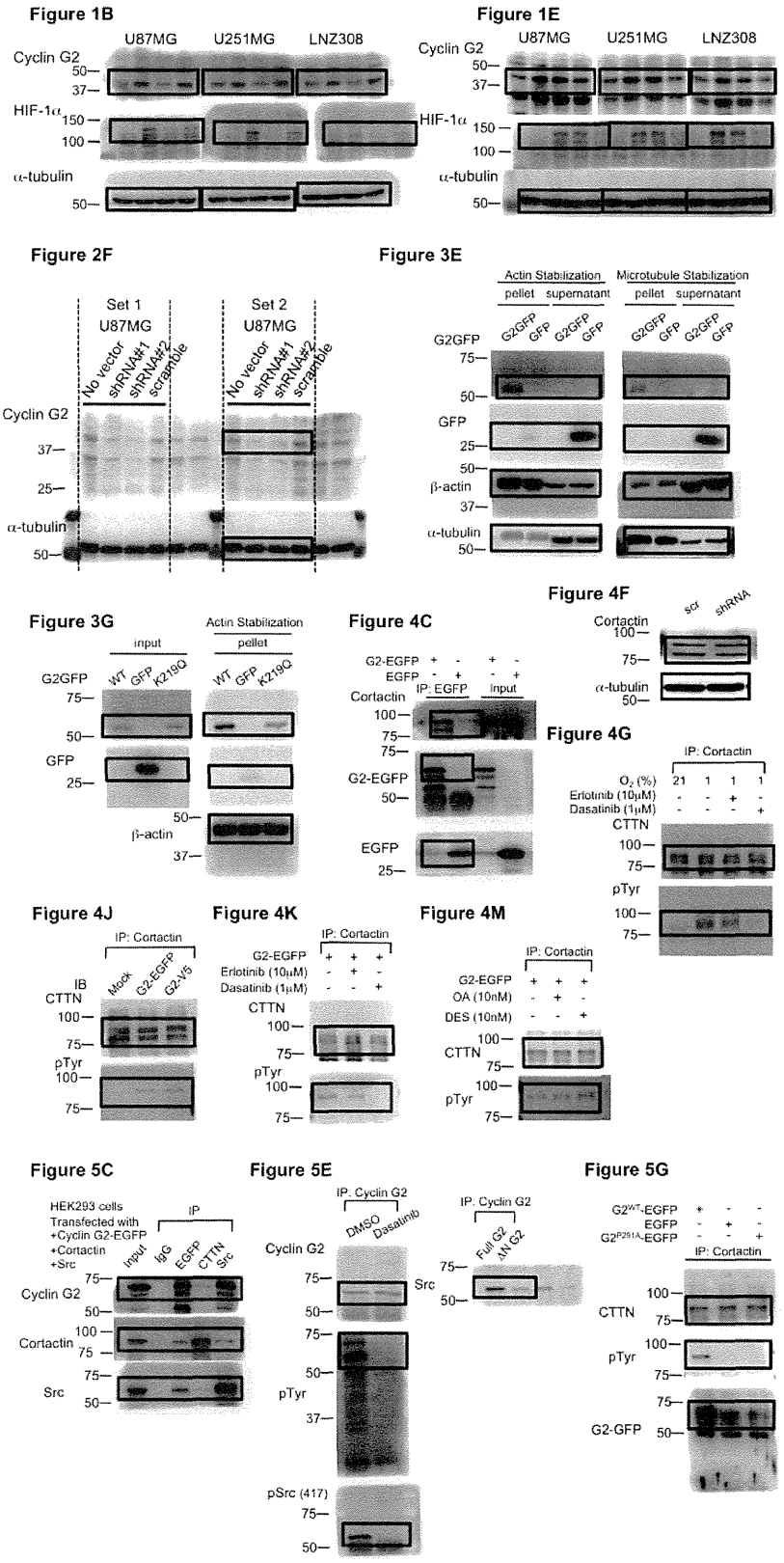

Figure W8. Full scans of the immunoblots shown in the figures. Boxes indicate the parts used in the figures, and numbers indicate the molecular weights. All data were obtained with the VersaDoc Imaging System (Bio-Rad).

Neurology & Neurophysiology

Moriuchi et al., J Neurol Neurophysiol 2013, 4:3
http://dx.doi.org/10.4172/2155-9562.1000159

Research Article Open Access

Use of 5-Aminolevulinic Acid to Detect Residual Meningioma and Ensure Total Removal while Avoiding Neurological Deficits

Shusuke Moriuchi[1*], Kimito Yamada[1], Makoto Dehara[1], Yoshifumi Teramoto[1], Takao Soda[2], Masami Imakita[3], Mamoru Taneda[1]

[1]*Departments of Neurosurgery, Rinnku General Medical Center, Izumisano, Osaka, Japan*
[2]*Departments of Neurology, Rinnku General Medical Center, Izumisano, Osaka, Japan*
[3]*Departments of 3Pathology, Rinnku General Medical Center, Izumisano, Osaka, Japan*

Abstract

5-Aminolevulinic acid (5-ALA) has been used successfully to resect meningioma without leaving a residual mass. The authors report their experience resecting meningiomas in 17 patients using 5-ALA. Except for one case, all meningiomas fluoresced intra-operatively under the microscope. Invasion to the dura mater, brain parenchyma, or skull showed fluorescence, allowing for confirmation of residual tumor; total removal of the meningioma could be performed more easily, and unexpected neurological deficits could be prevented by precise removal of the tumor under the microscope. With invasion to the dura mater or skull in one case, the extent of dural removal was decided by 5-ALA fluorescence with 1- to 2-cm safety margins. In another case with parenchymal invasion, close removal of the tumor without leaving residual tumor could be performed with 5-ALA fluorescence. With the above methods, no serious side effects or complications occurred in this study. Not all meningiomas fluoresced with 5-ALA, and 5-ALA is available for about 95% of meningiomas. 5-ALA appears easy to use and helpful for finding residual tumor and preventing recurrences by total removal of meningiomas.

Keywords: 5-ALA; Meningioma; Total resection

Introduction

Complete resection of meningiomas provides patients with the best chance for a cure; however, surgery is frequently difficult given the proximity of lesions to vital structures, such as cranial nerves, major vessels, and venous sinuses [1]. Accurate discrimination between tumor and normal tissue is crucial for optimal tumor resection. With the use of 5-aminolevulinic acid (ALA), meningiomas can be seen to fluoresce intra-operatively under the microscope [2]. Invasion to the dura mater, brain parenchyma, or skull shows fluorescence, allowing for confirmation of residual tumor, and total removal of the meningioma could be performed more easily, while unexpected neurological deficits could be prevented by precise removal of the tumor under the microscope. In the past 2 years, 17 total resections of meningiomas were performed using 5-ALA without recurrences and major complications, and it was found that fluorescence-guided resection may be beneficial for removal of complicated meningiomas that have a high risk of recurrence.

Methods

Patients' characteristics

A total of 17 consecutive patients (16 females, 1 male; average age, 65.5 years) undergoing resection of intracranial meningiomas from January 2011 to December 2012 were included in this study (Table 1). All of the meningiomas were histologically Grade I meningiomas. Tumor locations varied and included parasagittal, falx, sphenoid ridge, convexity, planum sphenoidale, and petroclival tumors. The sizes of the meningiomas ranged from more than 21 mm in diameter (Case 7) to a maximum of 76 mm in diameter (Case 2). In 4 of 17 cases, the middle meningeal artery feeding the meningioma was embolized preoperatively.

Preoperative and intraoperative procedures

After confirmation of normal liver function, patients were given 20 mg/kg of 5-ALA (Cosmo Oil Co., Ltd., Japan) 4 hours preoperatively [2,3]. Craniotomies were performed under general anesthesia. The meningiomas were confirmed using a 440-nm ultraviolet light source (violet-blue light), an optical component of the OPMI Pentero microscope (Carl Zeiss AG, Germany). Under the violet-blue light, the meningiomas showed charcoal-red fluorescence. Total removal of the meningiomas could be performed by resecting the tumor until the charcoal-red fluorescence could no longer be detected. In cases of proximity to vital organs, it is important to prevent damage to these organs and carefully remove the charcoal-red residual tumors.

Results

Tumor fluorescence

All 17 tumors were totally resected using 5-ALA fluorescence. No major neurological deficits were observed after surgery. The histopathological diagnosis of these 17 meningiomas was WHO grade 1 meningioma; the tumors' MIB-1 indices did not reach 5%. At the latest follow-up examination, 2 years after surgery, no patients showed evidence of recurrence. In 4 cases, the middle meningeal artery was embolized preoperatively. Even when the main feeding artery, the middle meningeal artery, was embolized, tumor fluorescence was strong in all cases. No correlation between preoperative embolization and tumor fluorescence was observed. Two cases (Case 4 and Case 5) showed weak tumor fluorescence. In Case 4, the tumor had intratumoral hemorrhage. The histopathological diagnoses were meningothelial meningioma with a MIB-1 index of 2% in Case 4 and transitional meningioma with a

***Corresponding author:** Dr. Shusuke Moriuchi, Departments of Neurosurgery, Rinnku General Medical Center, Izumisano, Osaka, Japan, Tel: 81-72-469-3111; Fax: 81-72-469-7929; E-mail: s-moriuchi@rgmc.izumisano.osaka.jp

Received June 21, 2013; **Accepted** July 29, 2013; **Published** August 05, 2013

Citation: Moriuchi S, Yamada K, Dehara M, Teramoto Y, Soda T, et al. (2013) Use of 5-Aminolevulinic Acid to Detect Residual Meningioma and Ensure Total Removal while Avoiding Neurological Deficits. J Neurol Neurophysiol 4: 159. doi:10.4172/2155-9562.1000159

MIB-1 index of 1% in Case 5. No correlation between size and tumor fluorescence was observed.

Representative cases

Case 3: A 37-year-old woman presented with headache and mild right hemiparesis. MR imaging showed a large meningioma (maximum diameter 59 mm) at the left parasagittal area, extending to the skull and causing the skull to bulge (Figure 1A). After craniotomy, it was found that the meningioma invaded into the inner layer of the skull and fluoresced charcoal-red (Figure 1B). The invasion of meningioma into the inner layer was drilled out until the charcoal-red light disappeared, and the skull was returned at closure. The parasagittal meningioma fluoresced strongly and was removed totally, and the attachment to the lateral wall of the superior sagittal sinus was coagulated (Figures 1C and 1D). The patient had no neurological deficit at discharge. The histopathological diagnosis was transitional meningioma with a MIB-1 index of 2%.

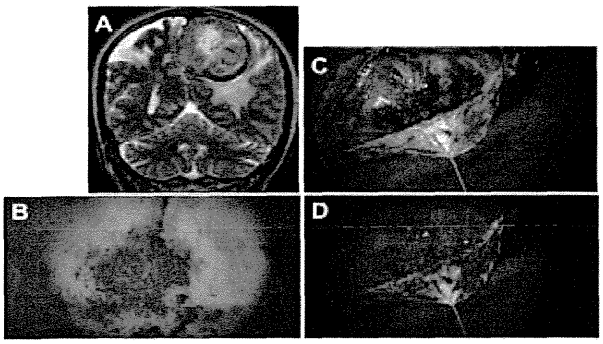

Figure 1: Case 3 of a 37-year-old woman with parasagittal meningioma. A: Preoperative T2-weighted MR image showing the large tumor with peritumoral edema that reached the superior sagittal sinus. B: Intraoperative photograph in the fluorescence mode of skull from intracranial side showing skull invasion of the tumor. C and D: Intraoperative photograph in the white-light mode of the surface of the main tumor mass after opening the dura mater (C), and the main tumor mass showed bright fluorescence in the fluorescence mode (D).

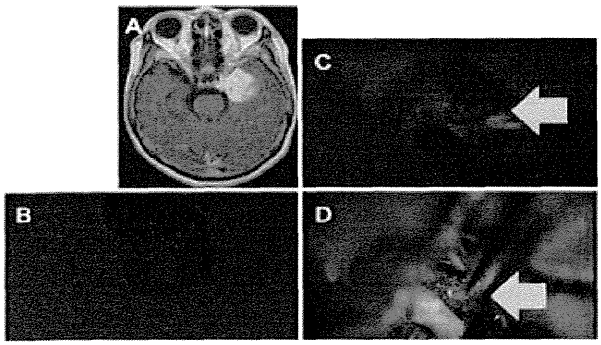

Figure 2: Case 4 of a 67-year-old woman with left sphenoid ridge meningioma. A: Preoperative gadolinium-enhanced T1-weighted MR image showing the main tumor with peritumoral edema. B: Intraoperative photograph in the fluorescence mode of the resected tumor showing some fluorescences. C and D: Intraoperative photograph in fluorescence mode of the tumor encased the left middle cerebral artery and invaded into the brain parenchyma showing fluorescence.

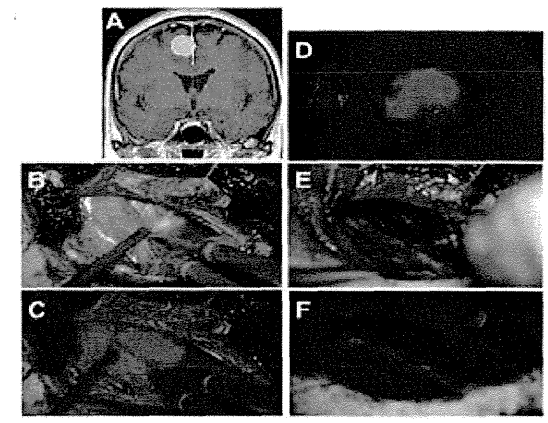

Figure 3: Case 10 of a 59-year-old woman of a right falx meningioma. A: Preoperative gadolinium-enhanced T1-weighted MR image showing the main tumor of right falx. B and C: Intraoperative photograph in fluorescence mode of the tumor showing bright fluorescence. D: The resected tumor (right) and the opposite side of the attachment of the resected falx (left) showed bright fluorescence. E and F: Intraoperative photograph in fluorescence mode of the falx coagulated showing no fluorescence.

Case 4: A 67-year-old woman presented with diplopia and headache. MR imaging showed a left sphenoid ridge meningioma with intratumoral hemorrhage and parenchymal edema adjacent to the tumor (maximum diameter 44 mm) (Figure 2A). The tumor encased the left middle cerebral artery and invaded into the brain parenchyma with charcoal-red fluorescence (Figures 2B and 2D). The tumor was resected totally until no fluorescence was observed. The patient had no neurological deficit and no epileptic seizures after operation. The histopathological diagnosis was meningothelial meningioma with a MIB-1 index of 2%.

Case 10: A 59-year-old woman presented with headache and mild weakness of the right lower extremity. MR imaging showed a right falx meningioma (maximum diameter 30 mm) (Figure 3A). The tumor showed strong charcoal-red fluorescence (Figure 3B-D). The falx attached to the tumor was coagulated, and the fluorescence disappeared (Figures 3E and 3F). After the attached falx was resected, the resected tumor and the opposite side of the falx to which the tumor was attached showed strong charcoal-red fluorescence (Figure 3D), showing that the meningioma invaded through the falx. The headache and weakness of the lower extremity disappeared after total resection. The histopathological diagnosis was transitional meningioma with a MIB-1 index of 2%.

Discussion

In this study, 5-ALA administration resulted in bright and diffuse tumor fluorescence in 15 (88%) of 17 cases, including the cases in which pre-operative embolization had been performed (Table 1). Protoporphyrin IX (PPIX) fluorescence was seen only in the main mass and areas of tumor invasion. In this series, the sensitivity and specificity of PPIX fluorescence of the main tumor mass were 88% (15 of 17 cases) and 100% (17 of 17 cases), respectively (Table 1). Fluorescence guidance allowed us to identify the extent of the tumor and helped us avoid leaving residual tumor tissue that was difficult to identify in the white-light mode. If we had not used fluorescence guidance, we might not have noticed several small areas of residual tumor showing 5-ALA fluorescence under violet-blue light with an operative microscope in

the operating room. In this study, numerous factors affected tumor recurrence: the tumor's soft consistency, lobular shape, encasement of the artery, invasion into the brain parenchyma, and dural attachment very close to the venous sinus, as well as bone invasion. Because of these factors, the risk of recurrence was considered very high [4-7]. It is worth noting that tumor remnants were identified by fluorescence in multiple regions. deVries and Wakhloo [8] reported that recurrent tumor is often found at multiple sites. Meningioma has a high risk of recurrence, and during excision, meningioma tissue can be left at any attachment to surrounding tissues, especially at attachments to the gliotic brain, major sinuses, the anterior visual pathway [9], and marginal dura mater. Aggressive excision of the dura and gliotic brain has been recommended to reduce this risk [7,10], but the optimal extent of dural resection has been controversial. Kinjyo et al. proposed a margin of 2 cm. Nakasu et al. reported that a 1-cm dural margin is insufficient to prevent recurrence [11,7]. The most suitable margin for dural excision will necessarily differ from case to case, because of differences in tumor growth rates and invasiveness. In light of these factors, photodynamic diagnosis may become a promising method of determining the extent of dural resection.

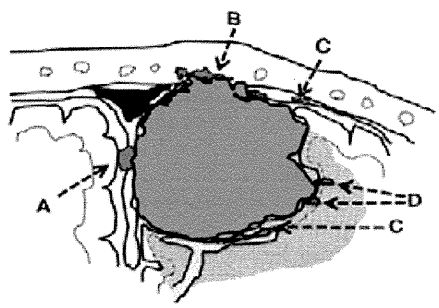

Figure 4: Schematic drawing showing areas most likely to harbor tumor remnants. A: Intradural invasion. B: Bone invasion. C: Dural extension. D: Tumor tissue behind vessels in the sulcus or parenchymal invasion. The gray zone shows the extent of the tumor. The texture close to the tumor shows the extent of brain edema.

On the other hand, indiscriminate excision can lead to complications related to brain and vascular injury. Therefore, if a tumor is located close to a major sinus, the skull base, or an eloquent area, then the excision of dura mater and brain tissue should be restricted to safe areas, and unresectable dura must be coagulated. Fluorescence guidance may help avoid unnecessary excision. The reasons why tumor remnants may be overlooked can be classified into three categories. 1) The tumor cells invade surrounding tissue, attached dura mater, bone, and brain, after which the invaded area is difficult to distinguish from the noninvaded area (Figure 4). 2) The tumor remnants may be hidden behind large vessels or the sinus, dural fold, or sulcus (Figure 4). 3) Daughter lesions may develop apart from the main mass. All three reasons can make tumor remnants difficult to identify with the naked eye or with the aid of a surgical microscope. The use of 5-ALA-induced fluorescence can help surgeons identify tumor remnants, because an area of strong red fluorescence will appear if even a small part of a remnant is present at the tissue surface. Fluorescence can make it easy to distinguish the one from the other and determine the extent of a given tumor.

In the present study, tumor invasion into the skull was also visualized by charcoal-red fluorescence. In most cases, hyperostosis in association with meningioma is related to tumor invasion. However, the extent of tumor invasion is difficult to judge from the appearance alone. Although it is relatively easy to treat bone invasion in cases of convexity meningioma, invasion at the skull base is hard to treat because it involves the cranial nerves, major blood vessels, and air sinuses. Therefore, the detection of bone invasion using photodynamic diagnostic methods would seem to be valuable, especially in surgery for skull-base meningiomas.

Many recent reports have described the usefulness of 5-ALA to identify the margin of a malignant tumor or glioma for maximal cytoreduction [6,12-16]. 5-ALA is an endogenous body metabolite central to heme biosynthesis that is readily absorbed and metabolized into porphyrins by malignant tumor cells (5). This phenomenon can aid in tumor resection to identify the residual tumor in tumor margins, when gross total resection is possible and desirable, with malignant cells fluorescing, allowing discrimination between tumor and normal functional brain tissue [6,12,13]. The side effects of 5-ALA are mild. Skin irritation, nausea, and transient elevation in liver function test

Case No.	Age, Sex	Tumor Location	Tumor Diameter(mm)	Tumor Fluorescence	Preoperative Embolization
1	62, F	rt PO parasagittal	44x40x46	Strong	No
2	62, F	rt F falx	76x49x67	Strong	Yes
3	37, F	lt FP parasagittal	59x58x50	Strong	Yes
4	67, F	lt sphenoid ridge	44x38x40	Weak	No
5	45, F	lt petroclival	28x14x24	Weak	No
6	65, M	rt P convexity	25x19x26	Strong	No
7	75, F	rt sphenoid ridge	21x21x20	Strong	No
8	65, F	lt sphenoid ridge	63x46x59	Strong	Yes
9	74, F	lt P convexity	40x40x46	Strong	No
10	59, F	rt P falx	30x25x21	Strong	Yes
11	75, F	planum sphenoidale	37x33x31	Strong	No
12	81, F	lt F convexity	41x29x28	Strong	No
13	60, F	rt petroclival	26x24x27	Strong	No
14	48, F	planum sphenoidale	22x19x20	Strong	No
15	60, F	rt F convexity	26x18x23	Strong	No
16	64, F	rt sphenoid ridge	32x26x26	Strong	No
17	48, F	lt FP parasagittal	42x32x26	Strong	No

Table 1: Characteristics of patients with meningioma. Abbreviations used in this table: M, male; F, female; PO, parieto-occipital; F, frontal; FP, fronto-parietal; P, parietal; rt, right; lt, left.

results have occurred in some adult patients given higher doses of 5-ALA [4,8,17,18]. Apart from transient nausea after dye ingestion, the present patients had no side effects, and their liver function tests were unchanged.

Accumulation in the normal central nervous system is restricted except in the subependymal zone and choroid plexus [18,19]. Many possible mechanisms have been posited to explain the selective accumulation of PPIX in neoplasms: (1) enhanced penetration of 5-ALA through the blood-brain barrier; (2) reduced transporter activity that drains PPIX outside of cells; and (3) reduced activity of ferrochelatase, which converts PPIX to heme [20]. At least one of these factors is probably involved in the strong 5-ALA-derived fluorescence in meningiomas. In general, there is no strict correlation between cell proliferation and PPIX accumulation. In meningiomas, the proliferation rate is relatively low [12].

In conclusion, applying this method to meningiomas that have a high risk of recurrence should be of value not only in ensuring that tumor remnants are not overlooked during resection but also in helping to avoid unnecessarily radical resection and the associated risk of morbidity. To confirm the usefulness of fluorescence-guided surgery for meningioma, further studies on its sensitivity, specificity, and effect on recurrence rates are needed.

Disclaimer

The authors report no conflict of interest concerning the materials or methods used in this study or the findings reported in this paper.

References

1. Samii M, Gerganov VM (2008) Surgery of extra-axial tumors of the cerebral base. Neurosurgery 62: 1153-1166.
2. Kajimoto Y, Kuroiwa T, Miyatake S, Ichioka T, Miyashita M, et al. (2007) Use of 5-aminolevulinic acid in fluorescence-guided resection of meningioma with high risk of recurrence. Case report. J Neurosurg 106: 1070-1074.
3. Moriuchi S, Yamada K, Dehara M, Teramoto Y, Soda T, et al. (2011) Use of 5-aminolevulinic acid for the confirmation of deep-seated brain tumors during stereotactic biopsy. Report of 2 cases. J Neurosurg 115: 278-280.
4. Al-Mefty O, Kadri PA, Pravdenkova S, Sawyer JR, Stangeby C, et al. (2004) Malignant progression in meningioma: documentation of a series and analysis of cytogenetic findings. J Neurosurg 101: 210-218.
5. Jääskeläinen J (1986) Seemingly complete removal of histologically benign intracranial meningioma: late recurrence rate and factors predicting recurrence in 657 patients. A multivariate analysis. Surg Neurol 26: 461-469.
6. Jääskeläinen J, Haltia M, Servo A (1986) Atypical and anaplastic meningiomas: radiology, surgery, radiotherapy, and outcome. Surg Neurol 25: 233-242.
7. Nakasu S, Nakasu Y, Nakajima M, Matsuda M, Handa J (1999) Preoperative identification of meningiomas that are highly likely to recur. J Neurosurg 90: 455-462.
8. de Vries J, Wakhloo AK (1994) Repeated multifocal recurrence of grade I, grade II, and grade III meningiomas: regional multicentricity (primary new growth) or metastases? Surg Neurol 41: 299-305.
9. Stafford SL, Perry A, Suman VJ, Meyer FB, Scheithauer BW, et al. (1998) Primarily resected meningiomas: outcome and prognostic factors in 581 Mayo Clinic patients, 1978 through 1988. Mayo Clin Proc 73: 936-942.
10. Salcman M (1991) Malignant meningiomas, in Al-Mefty O (ed): Meningiomas. New York: Raven Press, 75–86
11. Kinjo T, al-Mefty O, Kanaan I (1993) Grade zero removal of supratentorial convexity meningiomas. Neurosurgery 33: 394-399.
12. Iinuma S, Farshi SS, Ortel B, Hasan T (1994) A mechanistic study of cellular photodestruction with 5-aminolaevulinic acid-induced porphyrin. Br J Cancer 70: 21-28.
13. Kallio M, Sankila R, Hakulinen T, Jääskeläinen J (1992) Factors affecting operative and excess long-term mortality in 935 patients with intracranial meningioma. Neurosurgery 31: 2-12.
14. Morofuji Y, Matsuo T, Hayashi Y, Suyama K, Nagata I (2008) Usefulness of intraoperative photodynamic diagnosis using 5-aminolevulinic acid for meningiomas with cranial invasion: technical case report. Neurosurgery 62: 102-103.
15. Coluccia D, Fandino J, Fujioka M, Cordovi S, Muroi C, et al. (2010) Intraoperative 5-aminolevulinic-acid-induced fluorescence in meningiomas. Acta Neurochir (Wien) 152: 1711-1719.
16. Bekelis K, Valdés PA, Erkmen K, Leblond F, Kim A, et al. (2011) Quantitative and qualitative 5-aminolevulinic acid-induced protoporphyrin IX fluorescence in skull base meningiomas. Neurosurg Focus 30: E8.
17. Borovich B, Doron Y (1986) Recurrence of intracranial meningiomas: the role played by regional multicentricity. J Neurosurg 64: 58-63.
18. Ennis SR, Novotny A, Xiang J, Shakui P, Masada T, et al. (2003) Transport of 5-aminolevulinic acid between blood and brain. Brain Res 959: 226-234.
19. Olivo M, Wilson BC (2004) Mapping ALA-induced PPIX fluorescence in normal brain and brain tumour using confocal fluorescence microscopy. Int J Oncol 25: 37-45.
20. Peng Q, Warloe T, Berg K, Moan J, Kongshaug M, et al. (1997) 5-Aminolevulinic acid-based photodynamic therapy. Clinical research and future challenges. Cancer 79: 2282-2308.

Citation: Moriuchi S, Yamada K, Dehara M, Teramoto Y, Soda T, et al. (2013) Use of 5-Aminolevulinic Acid to Detect Residual Meningioma and Ensure Total Removal while Avoiding Neurological Deficits. J Neurol Neurophysiol 4: 159. doi:10.4172/2155-9562.1000159